ELSEVIER

Nuclear Instruments and Methods in Physics Research A 443 (2000) 557–577

NUCLEAR INSTRUMENTS & METHODS IN PHYSICS RESEARCH Section A

www.elsevier.nl/locate/nima

# A high-resolution $BaF_2$ positron-lifetime spectrometer and experience with its long-term exploitation

F. Bečvář[a,]*, J. Čížek[a], L. Lešťák[a,1], I. Novotný[a], I. Procházka[a], F. Šebesta[b]

[a]*Charles University in Prague, Faculty of Mathematics and Physics, V Holešovičkách 2, CZ-180 00 Prague 8, Czech Republic*
[b]*Czech Technical University, Faculty of Nuclear and Physical Engineering, Břehová 7, CZ-115 19 Prague 1, Czech Republic*

Received 18 May 1999; received in revised form 27 September 1999; accepted 15 October 1999

## Abstract

A spectrometer for measuring positron lifetimes in solids is described. It consists of a pair of $BaF_2$ scintillators coupled to Philips photomultipliers XP2020Q and a fast-slow coincidence system composed of standard NIM modules. To achieve adequate stability and the maximum performance of the spectrometer, several improvements on commonly used techniques have been introduced. Of these, modified dynode timing based on the utilization of the negative, "anode-like" fast signal seems to be the most important. At a typical rate of 35–40 coincidences/s, the best recorded timing resolution power of the spectrometer for a $^{22}$Na positron source amounted to 139 ps. Although the photomultipliers used display marked effects of ageing on their dynode systems, the timing resolution of the spectrometer after running for more than five years has deteriorated to only 146 ps. This long-term behaviour has been achieved as a result of measures for compensating the influence of the gradual loss of photomultiplier gain. Important details relating to the spectrometer design, as well as to its optimization and testing, are given. Examples of measured positron-lifetime spectra are given to demonstrate the performance of the spectrometer. The rich data relating to the long-term behaviour of the spectrometer are broadly discussed. © 2000 Elsevier Science B.V. All rights reserved.

*PACS:* 78.70.Bj

*Keywords:* Positron annihilation in solids; Positron-lifetime spectrometer; Fast–slow coincidence system; $BaF_2$ scintillation detectors; Timing resolution

## 1. Introduction

Positron-lifetime spectroscopy proved itself to be a powerful experimental method in solid-state physics and materials science [1]. After a development that ended approximately in the middle of the 1980s, it virtually reached the present state-of-the-art and acquired an almost standard form. The last of its crucial innovations were represented by the introduction of the $BaF_2$ scintillators [2–4] and the dynode timing [2,5]. Although positron-lifetime spectroscopy has become widely recognized, it still suffers from persistent problems. Of these, the limited timing resolution power and gradual worsening of this important parameter due to the ageing of photomultipliers and $BaF_2$ crystals seem to be the most serious. While the optimization of the timing

---

* Corresponding author Tel.: + 420-2-2191-2566; fax: + 420-2-2191-2567.

*E-mail address:* becvar@mbox.troja.mff.cuni.cz (F. Bečvář)

[1] Deceased.

0168-9002/00/$ - see front matter
PII: S0168-9002(99)01156-0

resolution has been addressed in several previous papers, see e.g. Refs. [2,4,6–10], the literature related to the equally relevant problems of ageing and ways to cope with them is, as far as we know, still missing. The lack of such information is felt strongly, especially in the context of the previously reported positron-lifetime spectrometers in Refs. [6–8] which, displayed excellent timing characteristics. In this respect, the most remarkable results have been achieved with the spectrometer reported in Ref. [6] that was based on the use of Hamamatsu R2083Q photomultiplier tubes (PMTs) in combination with $BaF_2$ scintillators. The timing resolution, expressed in full-width at half-maximum (FWHM) of the timing response function, was equal in this case to $140 \pm 1$ ps for $^{22}$Na. In Refs. [7,8] for a spectrometer, assembled from Philips XP2020Q PMTs, $BaF_2$ scintillators and specially developed electronics modules, a value of FWHM equal to $165 \pm 1$ ps was reported. Unfortunately, no data that would demonstrate the routine use of these spectrometers in positron-lifetime experiments are available.

This paper deals with the positron-lifetime spectrometer installed at Charles University in Prague. While designing this instrument we took into account virtually all the available expertise in the given field and made additional improvements to achieve a superior timing resolution and optima in other characteristics. Moreover, the design respected an important requirement that all the sophisticated components of this spectrometer be commercially available. Compared to an earlier report about the same spectrometer [11] the present paper gives its exhaustive description and describes its optimization. In addition, it includes an account of the five-year continuous utilization of this instrument. Some measures for slowing-down the effects of ageing and for their compensation are also reported.

## 2. Principles and requirements of positron-lifetime spectroscopy

In a conventional positron-lifetime experiment, the radioactive isotope $^{22}$Na is used as a source of the positrons. In this case, the emission of 99.93% of positrons is accompanied by a 1274 keV $\gamma$ transition in the daughter nucleus $^{22}$Ne. The emitted positrons enter the material studied where, typically within a period of several picoseconds, they are moderated down to thermal energies and eventually annihilate, each emitting a pair of annihilation $\gamma$ rays with energies of 511 keV. A spectrum of time differences between detecting the 511 and 1274 keV $\gamma$ rays, called hereafter the delayed-coincidence spectrum, is measured. By analysing this spectrum information about the lifetimes $\tau_i$ and the intensities $I_i$ of various groups $i$ of positrons annihilating in a given material can be deduced.

In fact, each individual lifetime is represented in the delayed-coincidence spectrum not by a mere exponential component, but by a convolution of the exponential function with the timing response function of the spectrometer. The resolution power, characterized by the narrowness of the timing response function, and the maximum achievable delayed-coincidence counting rate are the most important factors that limit the ability of positron-lifetime measurements in identifying and resolving positron-lifetime components in the spectrum. The resolution power of the best existing positron-lifetime spectrometers is characterized by the FWHM values of which are still higher than positron lifetimes for defect-free metallic systems, i.e. 100–160 ps, or at most comparable with these lifetimes. As far as defected metallic systems are concerned, the lifetime of positrons in the free state can be as short as several tens of ps. It is thus evident that any improvement in timing resolution is of major importance while studying positron annihilation in metals.

## 3. Description of the spectrometer and other details

### 3.1. Detectors

The detector part of the spectrometer consist of two $BaF_2$ cylindrical crystals with dimensions $\varnothing 25$ mm × 10 mm mounted on fast, quartz-window PMTs. The crystals were purchased from the Karl Korth Kristalle GmbH, Kiel, Germany. Philips PMTs, Model XP2020Q, with a photocathode diameter of 51 mm were chosen. Initially, in 1992, we used a pair of these PMTs that were manufactured in 1991 (Serial Nos. 40432 and 40436). The values of *the photocathode blue sensitivities* of these PMTs were 10 μA/1 mF, the meaning of this quantity being fully specified in Ref. [12]. After four months of testing and running the spectrometer we replaced the PMTs for another pair of the same model, but manufactured before 1986 (Serial Nos. 15553 and 15563). In this case *photocathode radiant sensitivities* at 401 nm were declared by the manufacturer for these PMTs to be 80 and 77 mA/W, respectively.

The crystals were polished using the procedure described in Ref. [13]. Following a recommendation of the Darmstadt group [14], the front and side surfaces of the crystals were coated with seven layers of PTFE (Teflon) tape with a thickness of 38 μm and a pore size of 0.22 μm. The wrapped crystals were encapsulated in duralumin cups, as shown in Fig. 1. Each crystal was optically coupled to the quartz window of a PMT using immersion, represented by about 5 mm$^3$ of silicon grease of the maximum acceptable viscosity. The PMT and the encapsulated crystal are sealed in a common duralumin water-proof housing. Inside the housing there is about 25 cm$^3$ of silica-gel to enhance the protection of the crystal against moisture. In order to prevent the photocathode of the PMT from electrolytic destruction, the crystal and the quartz window are electrically well insulated from the housing. Further details are shown in Fig. 1. The zero magnetic field at the sites of PMTs is ensured by a pair of compensating Helmholtz coils with a diameter of 700 mm, see Fig. 2. In fact, in 1995 these coils replaced the permalloy magnetic shielding, formed by two cylinders with a diameter and length of 61 and 50 mm, respectively, which we used in the earlier version of the spectrometer [11]. In order to reach the maximum possible compensation of the local magnetic field, all parts of the spectrometer were made of non-magnetic materials.

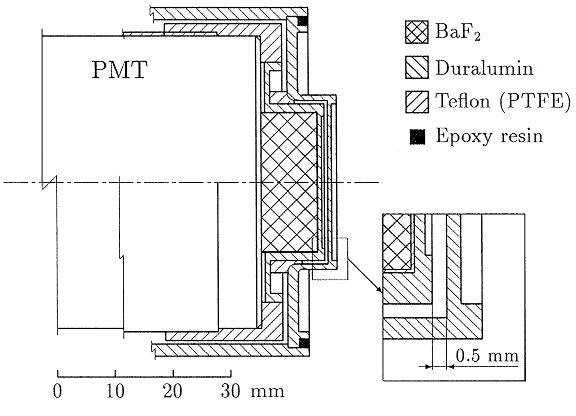

Fig. 1. Assembly of the $BaF_2$ crystal and the PMT, including their common housing and other details.

As seen in Fig. 2 and schematically in Fig. 3, a face-to-face detector geometry with a common symmetry axis was chosen. In order to minimize parasite effects due to simultaneous detections of both 511 keV photons [4,15] and to simultaneously keep a sufficiently high coincidence count rate, the assembly of the positron source and the samples is located in between the $BaF_2$ crystals, out of the common axis at a radial distance slightly greater than the radius of the crystals, see Fig. 3. With such geometry, thanks to a strict angular anticorrelation of each pair of annihilation $\gamma$ rays, only one of these two $\gamma$ rays may form together with the 1274 keV $\gamma$ ray an event of a delayed coincidence. However, to be strict, this is not true for much less probable cases when the Compton scattering of these annihilation $\gamma$ rays with surrounding material occurs prior to their detection. From the point of view of a maximum coincidence count rate it is important that for the geometry shown in Fig. 3 there exists an optimum separation between the faces of the crystals. For the given crystals this separation is approximately 14 mm.

### 3.2. High-voltage dividers

In an attempt to reach the optimum performance of the spectrometer we gradually tested four types of high-voltage (HV) dividers referred to hereafter as I–IV. Their common scheme is seen in Fig. 4. Their selection was guided by our previous experience with a provisional version of the spectrometer. These HV dividers differ from each other only in the voltage distribution along the dynode chain, as shown in Table 1. The first three were examined in conjunction with the PMTs of later production

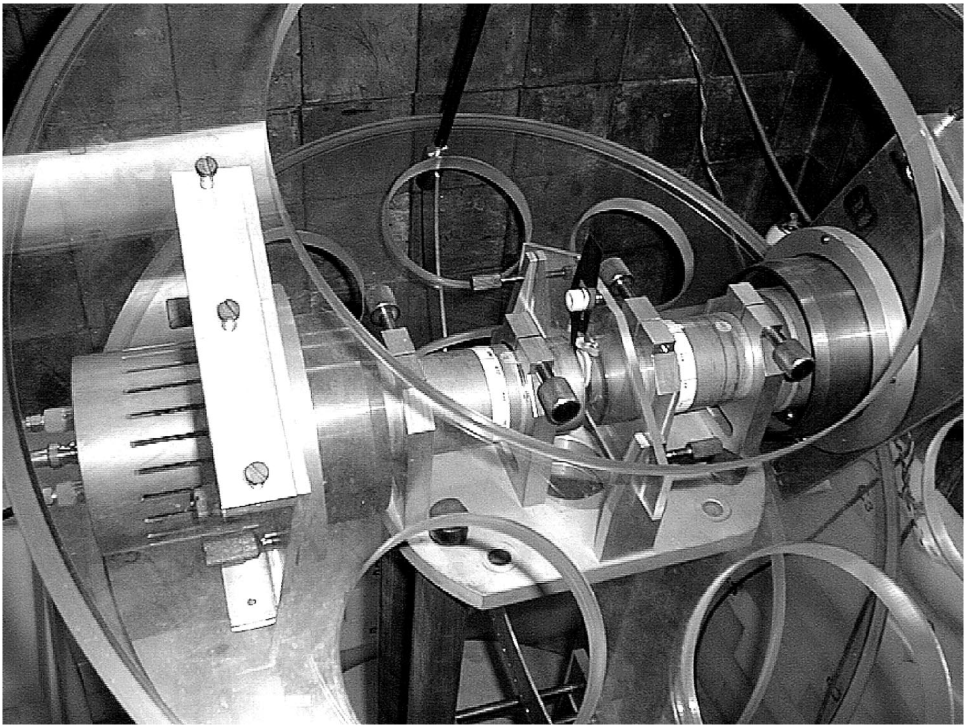

Fig. 2. A view of the detector part of the positron-lifetime spectrometer. Both detectors, the Helmholtz compensating coils, the holder of the sample and the table for mounting a cryostat are seen.

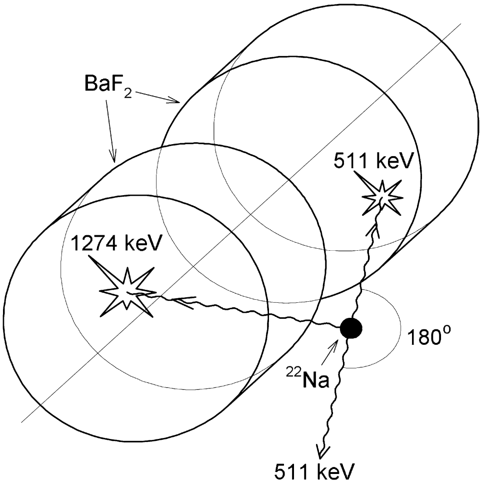

Fig. 3. The configuration of the positron source and the scintillation crystals.

(Serial Nos. 40432 and 40436), while the HV divider IV has been used exclusively in combination with the older PMTs (Serial Nos. 15553 and 15563).

The schematic diagram of the HV divider IV together with a simple passive RC circuit for shaping the output signals is shown in Fig. 4. Under scrutiny it can be seen from Table 1 that all the HV dividers differ significantly in several respects from what has been recommended by the manufacturer of the PMTs [12]. Specifically, the voltage applied between the dynode D2 and the photocathode is increased to exceed slightly a maximum permissible value, while inter-dynode voltages at the end of the dynode chain are suppressed. In addition, to reach a maximum timing resolution, the fast signal is extracted not from the anode, as usual, but from the dynode D10, as first recommended in Ref. [16]. In this mode of operation the dynode D11 plays the role of a grounded anode, the ground potential

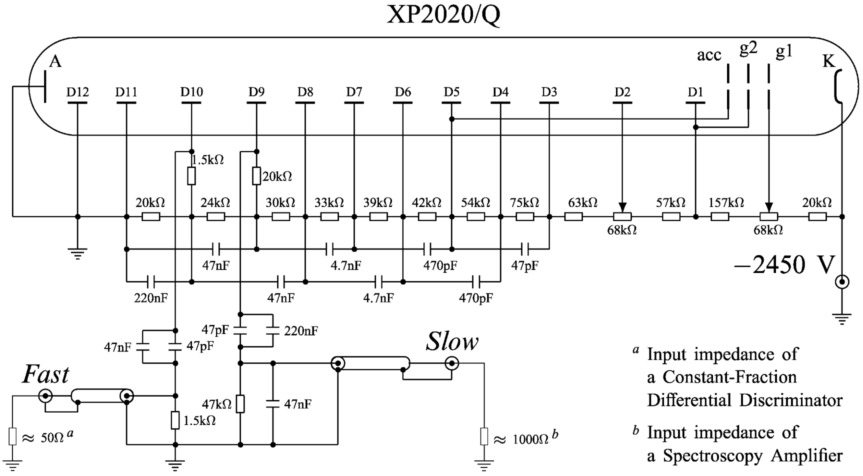

Fig. 4. The common scheme of the examined HV dividers. The values of resistance shown belong to the divider IV specified in Table 1.

Table 1

Voltage differences at various pairs of PMT electrodes for four voltage dividers I–IV mentioned in the main text. The values of these differences are expressed in units $U_0$, representing the average voltage difference at pairs D6–D7 and D7–D8. Total absolute voltages applied are also listed

| | Voltage difference in units $U_0$ | | | |
|---|---|---|---|---|
| Pair of electrodes[a] | Divider I | Divider II | Divider III | Divider IV |
| A–D12 | 0.00 | 0.00 | 0.00 | 0.00 |
| D12–D11 | 0.00 | 0.00 | 0.00 | 0.00 |
| D11–D10 | 1.43 | 1.43 | 1.43 | 0.56 |
| D10–D9 | 1.44 | 1.44 | 1.43 | 0.67 |
| D9–D8 | 1.00 | 1.00 | 2.06 | 0.84 |
| D8–D7 | 1.00 | 1.00 | 1.00 | 0.92 |
| D7–D6 | 1.00 | 1.00 | 1.00 | 1.08 |
| D6–D5 | 1.00 | 1.00 | 1.00 | 1.17 |
| D5–D4 | 1.73 | 1.74 | 1.35 | 1.48 |
| D4–D3 | 2.77 | 2.66 | 2.97 | 2.07 |
| D3–D1 | 7.08 | 7.19 | 7.62 | 5.23 |
| D2–D1 | Adjustable | Adjustable | Adjustable | Adjustable |
| D1–K | 9.63 | 9.02 | 9.01 | 7.17 |
| g1–K | Adjustable | Adjustable | Adjustable | Adjustable |
| D11–K | 28.08<br>(2500 V) | 27.48<br>(2500 V) | 28.07<br>(2500 V) | 21.19<br>(2450V) |

[a] Manufacturer's labelling, see Ref. [14].

being also kept on the true anode and the dynode D12.

All HV dividers were assembled in a compact form of printed-circuit boards soldered directly onto PMT sockets. All connections were made as short as possible to minimize reflections and interference of PMT signals inside the HV divider housing. For the same purpose the fast and slow signals at the output connectors are led from the printed-circuit board of the HV divider by short coaxial cables inside the metallic divider housing. However, in order to rule out radio-frequency (RF) cross-talks *between two detectors*, it is important that the outer sleeves of the output connectors be grounded to the divider housing, otherwise small but significant wave structures in the delayed-coincidence spectra may occur. For insulated connector sleeves such structures do indeed appear. In this case, we have proved uniquely that they result from the RF signal radiated by the gap between the connector sleeve and the housing of one detector with the subsequent reception of this signal by a similar gap at the other detector and vice versa. Following our expectation the time dependence of these structures in those parts of the delayed-coincidence spectra, where random background is dominating reproduces approximately the shape of *the time derivatives* of the transmitted RF signals.

### 3.3. Electronics

A principal scheme for the hardware processing of detector signals, as well as for accumulating and monitoring the raw data are shown in Fig. 5. The configuration of electronics modules shown here is conventionally referred to as the "fast–slow" arrangement.

The timing signal from the dynode D10 of each detector passes to the input of a Constant-Fraction Differential Discriminator (CFDD), ORTEC Model 583. In the case of HV dividers I, II and III, we first inverted the fast signal with the aid of the inverting transformer, ORTEC Model IT100, and

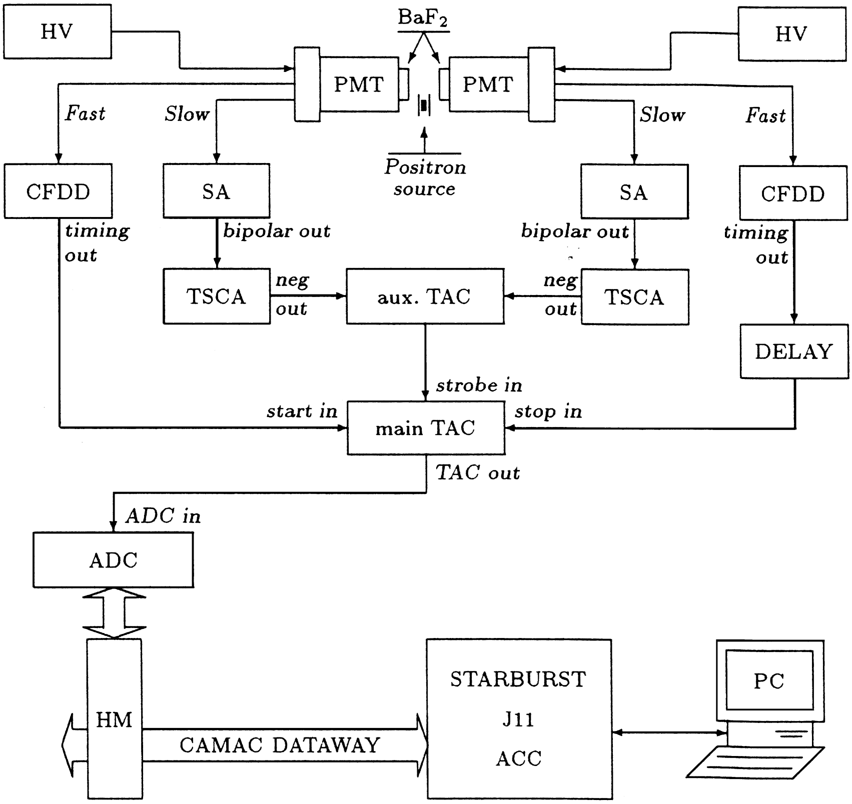

Fig. 5. The principal scheme of the signal processing and data acquisition system. Abbreviations of the individual modules are given in the text if not self-explanatory.

then we used it to feed the CFDD. However, initial testing measurements indicated that to reach the maximum timing resolution power, the factory built-in constant fraction attenuation factor $f = 0.2$ in the ORTEC Model 583 CFDD was not an optimum choice. It also turned out that to obtain the maximum resolution the CFDDs required a clipping time that would be appreciably lower than the minimum clipping time of 0.9 ns adjustable with the external cable on a given Model 583. To bypass these difficulties we split the inverted fast signal to feed two inputs: the "regular" input of the CFDD, and the input of the CFDD that is normally fed by the output end of the external clipping cable. The idea behind our trick is elucidated by the scheme shown in Fig. 6. It is evident that by changing the difference of cable lengths $l_1$ and $l_2$ one can chose *any clipping time*. Besides that, by changing the ratio of resistances $R_1/R_2$ and fixing their product $R_1R_2$ at the value of the square of the characteristic impedance, i.e. $Z_0^2 = 2500\ \Omega^2$, any value of the constant fraction attenuation factor can be reached. The fixed value of the product $R_1R_2$ is required to prevent undesirable reflections of the fast signal. The only disadvantage of this "non-destructive" change of the built-in constant fraction attenuation factor is a somewhat reduced sensitivity of the CFDD.

At present, when the HV divider IV is used, no pulse inversion is needed, as the leading edge of the fast voltage signal displays a well-expressed negative slope, capable of exciting the CFDD, in a similar way as a genuine anode signal. In the case of the HV divider IV the shape and absolute size of the fast detector signal is shown in Fig. 7. Both CFDDs are operating in the constant fraction mode with the factory built-in constant fraction attenuation factor. In view of the relatively low value of the fast signal the above-outlined method for non-destructive modification of the built-in constant fraction factor of the CFDDs could not be applied. The minimum adjustable CFDD clipping time, provided by the external cable on both CFDDs, was found to ensure the best timing resolution. Additional reduction of the clipping time, achieved by shortening the cables inside the CFDD modules, did not bring any further improvement of the resolution. The combination of the older PMTs

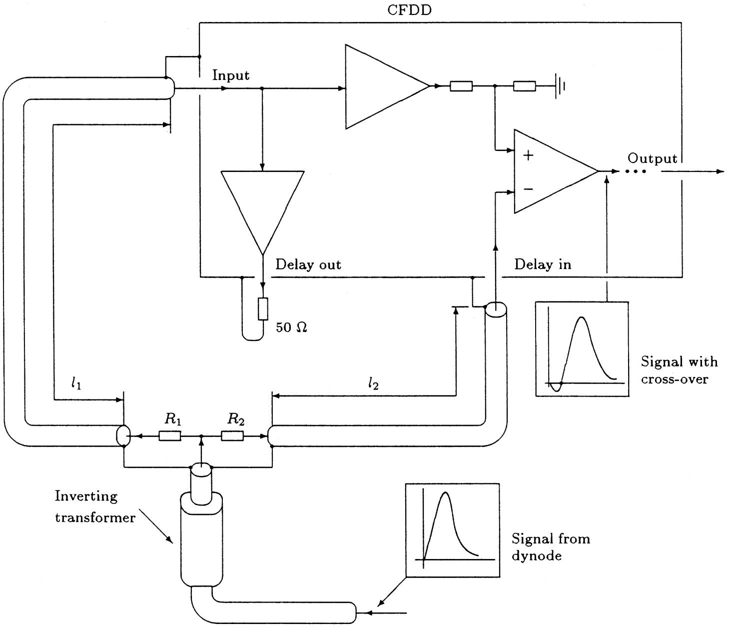

Fig. 6. A simplified block scheme explaining the idea of the non-destructive method for changing the constant-fraction attenuation factor of CFDDs.

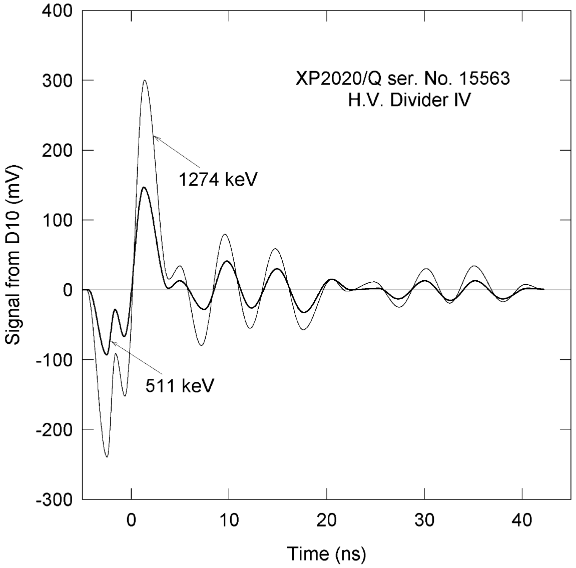

Fig. 7. The fast signal from the 10th dynode of an XP2020/Q PMT for $\gamma$-ray energies of 511 and 1274 keV as observed in March 1999 on a 250 MHz oscilloscope. The high voltage applied was $-2500$ V.

with the HV divider IV has been continuously used since 1993. During this period irreversible changes on the surfaces of the dynodes appeared and the gain of the PMTs gradually decreased up to the point when the fast signal from the stop detector became critically small and could not be properly processed by the CFDD. The factor of the overall decrease of the fast signal from the PMTs over the period of 4.3 yr was estimated to be 0.25, while the slow signal decreased approximately by a factor of 0.09. Together with these changes some worsening of the timing resolution of the spectrometer has been observed. As a remedy, a Hewlett–Packard MMIC high-frequency pre-amplifier, Model MSA-0404 with a gain of 7.5 dB and an upper frequency limit of 2.7 GHz was installed in the middle of 1997 to provide amplification of the fast signal from the stop detector. Later this amplifier was removed and a pair of Hewlett–Packard amplifiers, Model MSA-0204 with a gain of 11 dB and an upper frequency of 1.8 GHz were used to enhance the fast signals from *both* detectors; these amplifiers are fed by the PMT fast outputs and provide the input signals for the CFDDs. Because the signal was inverted by these amplifiers, the inverting transformer, ORTEC Model IT100, was used to restore the original polarity of the signal. Each CFDD performs a coarse energy selection of the corresponding photopeak region. Timing signals from the CFDDs are led to the start and stop the inputs of the TAC, ORTEC Model 567, denoted as the "main TAC" in Fig. 5.

As can be seen from Fig. 4, the slow signal from the detectors is first shaped by a passive RC-integration circuit with $\tau \simeq 50$ μs. Then, as shown in Fig. 5, the signal proceeds to a Spectroscopy Amplifier (SA), CANBERRA Model 2020, operated at the shortest shaping time (0.25 μs) to suppress the effects of pile-up. The bipolar outputs from the SAs are led to the timing single-channel analysers (TSCAs), ORTEC Model 551, adjusted to appropriate $\gamma$-ray energy windows. The negative output pulses from the TSCAs pass to the start and stop inputs of the auxiliary TAC which serves as a slow-coincidence unit generating the strobe signal for the main TAC. The output pulses from the main TAC are digitized by an Analog-to-Digital Converter (ADC), CANBERRA Model 8077, whose data output is connected to a Histogramming Memory (HM), C.E.S. Model HM2161, controlled via a CAMAC dataway by the C.E.S. ACC2180 STARBURST J11 Auxiliary Crate Controller (ACC).

With our adopted compact detector–source geometry the most critical factor that reduces the number of recorded events per unit of time in the delayed-coincidence spectra is the considerable dead time of the TSCA that selects the 511 keV $\gamma$ line. In order to bypass this difficulty, in the mid 1998s we modified the slow branches of the electronics system in the way shown in Fig. 8. Instead of a separate selection of energies deposited in the two detectors, the modified system accepts only those events for which the sum of these energies falls within a suitably chosen energy interval centered around the value $511 + 1274$ keV. The energy summation is provided by connecting both output signals from dynodes D9 to the input of the SA. It is tacitly assumed that the responses of both detectors to the deposited $\gamma$-ray energies in them are equal. This condition can easily be observed by

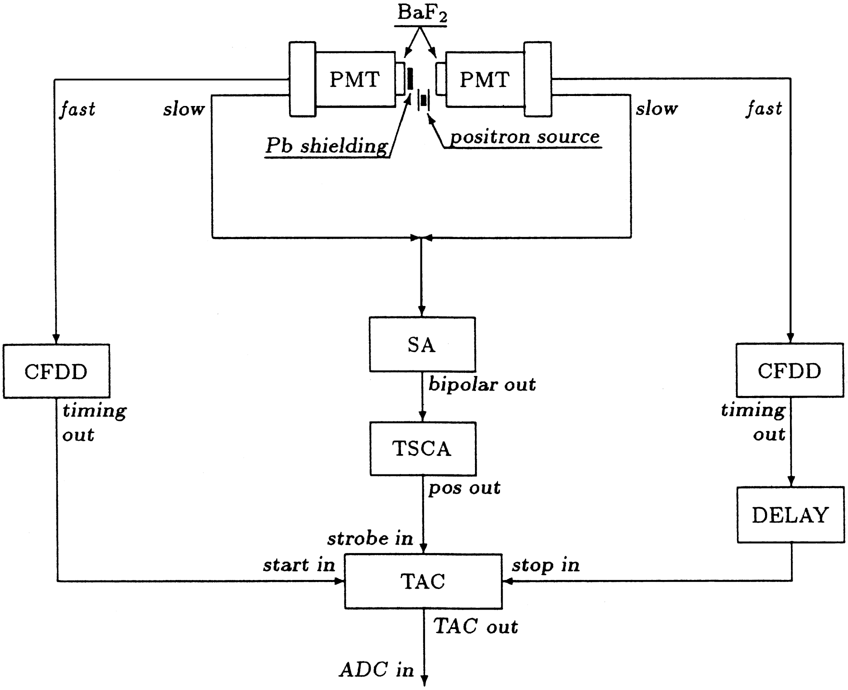

Fig. 8. A modification of the electronics system for the regime of strobing the TAC by a signal derived from the $\gamma$-ray energy sum.

careful adjustment of the high voltages applied to the PMTs. More details on the modified energy selection of coincidence events are given elsewhere [17].

### 3.4. Positron source

Positron sources, used in the routine measurements with our spectrometer, are prepared by depositing and sealing $\simeq 1.3$ MBq of $^{22}$NaCl between two mylar-type D clear films manufactured by Du Pont de Nemours of thickness $\sim 2$ μm. The assembling sequence is schematically shown in Fig. 9. Carrier-free $^{22}$NaCl in aqueous solution, purchased from Amersham Life Science, is used. Desired amount of activity is extracted by means of a micropipette from a stock solution with a specific activity of 1–9 MBq/ml into a Teflon dish in which it is evaporated to a volume 1–2 μl by an infra-red lamp. A drop of this concentrated solution is put using a micropipette at the centre of a circular piece of the supporting foil and is gradually dried for 15 min using the infra-red lamp. Subsequently, it is covered with another foil of the same kind and sealed with the aid of rings cut from a thin selfadhesive Scotch tape. The diameter of the radioactive spot is always less than 3 mm. As a result of radiation damage the mylar foils gradually become brittle and sooner or later leakage of radioactivity occurs, which restricts the lifespan of positron sources to typically 6 months.

### 3.5. Data acquisition and analysis

During long-term measurements drifts of time zero of the measured spectrum would cause its spreading. To avoid this deterioration the delayed-coincidence spectrum is created from a large number of separate measurements. In each of them, lasting typically 30 min, a *partial* delayed-coincidence spectrum is accumulated in the HM. The length of partial spectra amounts to 8192 channels with an average channel width of 3.13 ps. The time

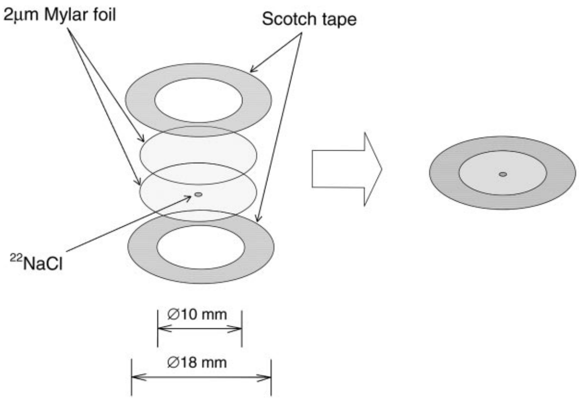

Fig. 9. Sealing a positron source.

scale is thus fine enough to make corrections for time-zero long-term drifts during data acquisition with the aid of a simple shift of a partial spectrum by an integer number of channels. The size of this shift is given by the difference between the actual position of some pre-defined reference point in the spectrum and the required position of that point. For this purpose the given partial spectrum is shifted by a *fixed* number of channels and then it is subtracted from the original, not the shifted spectrum. The reference point is then determined as the number of the channel at which the difference spectrum crosses zero. In fact, the reference point is taken as the cross-over point of the regression line that locally approximates the difference spectrum in the vicinity of its crossing zero. This way of determining the reference point is important for minimizing statistical uncertainties, associated with the limited number of counts in partial spectra. The sum of the shifted partial spectra is accumulated in RAM, stored onto a hard disk and eventually transferred to a PC for further off-line analysis in which the delayed-coincidence spectra are decomposed into their individual components by means of an unscrambling procedure [18] based on the maximum-likelihood method.

## 4. Optimization and testing

Following our testing measurements, the optimum voltages between the pairs of electrodes D2-K and g1-K that are needed to get the best timing resolution simultaneously yield the maximum slow-output signals. Owing to this ascertainment the focussing voltages of PMTs could easily be adjusted.

It turned out that the permalloy magnetic shielding, used in the earlier setup of the spectrometer, was not efficient enough. Besides that, the photocathodes proved to be inhomogeneous as far as quantum efficiency and/or electron collection time are concerned. Furthermore, as explained in Section 3.1, the sandwich, formed by the positron source and the sample, has to be located out of the common axis of the detectors. All these circumstances make the timing resolution power sensitive not only to the rotation angles, $\Phi$ and $\Psi$, of the detectors around their axis, but also to the rotation angle, $\Theta$, of the sandwich around the same axis. It has been found that the FWHM, characterizing the timing response function, depends on $\Phi$, $\Psi$ and $\Theta$ in a complicated way, when the minimum FWHM with respect to one parameter, say $\Theta$, at fixed values $\Phi_0$ and $\Psi_0$ of the remaining parameters depends on these fixed values. The procedure of minimizing the FWHM could not thus be done by three *independent* acts of minimization with respect to angles $\Theta$, $\Phi$ and $\Psi$, i.e. relatively large number of points in the 3D space $\Phi \times \Psi \times \Theta$ is needed. The problem of finding the optimum angles $\Phi$, $\Psi$ and $\Theta$ became simple when a full compensation of the magnetic field was achieved by the use of Helmholtz coils. In this case it was enough to fix the angle $\Theta$ at an arbitrary value and find a minimum FWHM in the 2D space $\Phi \times \Psi$. Finding the minimum in such a space is simple, as it consists of two *independent* steps in which the minimum is first sought with respect to one of the angles $\Phi$ and $\Psi$ and then with respect to the other. For the sake of convenience the optimization of angles $\Phi$ and $\Psi$ was performed with the aid of the measurement of delayed-coincidence spectra for the $\gamma$ cascade following the decay of $^{60}$Co. As can be deduced from the data in Fig. 10, for the full 2D range of angles $\Phi$ and $\Psi$ the value of FWHM varies within an interval of 104.5–126.5 ps. As is apparent, this interval is relatively broad, which justifies the real need for the optimization of $\Psi$ and $\Phi$.

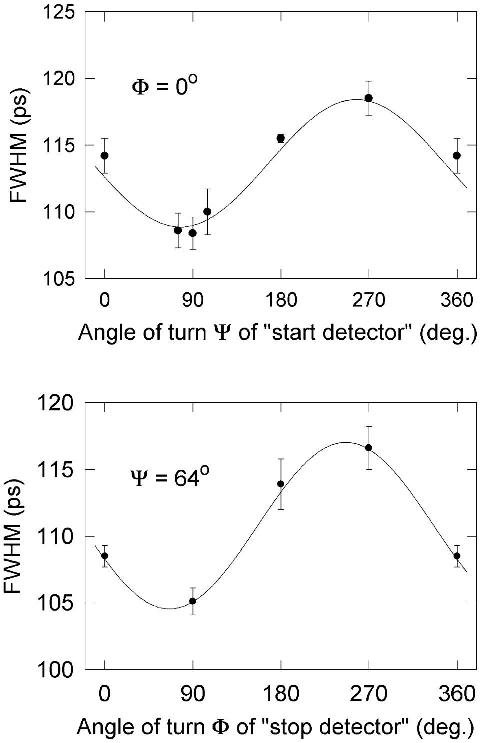

Fig. 10. Values of FWHM of spectrometer response function, determined from measurements with $^{60}$Co, as functions of angles of turn $\Psi$ and $\Phi$ of start and stop detectors, respectively. The data shown were obtained when the magnetic field at the site of photocathodes and dynodes was fully compensated with the aid of Helmholtz coils.

Assuming that the uncertainty in the timing of a *single* detector is proportional to $N_{\mathrm{pe}}^{-1/2}$, where $N_{\mathrm{pe}}$ is the number of emitted photoelectrons, the following proportionality holds for the value of FWHM of the spectrometer:

$$\mathrm{FWHM} \sim \left(\frac{1}{E_{\gamma 1}} + \frac{\alpha^2}{E_{\gamma 2}}\right)^{1/2} \tag{1}$$

where $E_{\gamma 1}$ and $E_{\gamma 2}$ are the energies of $\gamma$ rays detected by the first and the second detector, respectively, while $\alpha$ is a parameter characterizing the uncertainty in timing of the second detector relative to that of the first one. From our previous $^{22}$Na measurements with the interchanged detectors, when $E_{\gamma 1} = 1274$ keV and $E_{\gamma 2} = 511$ keV, we got a value of FWHM that was higher by a factor of 1.19 compared to the case when $E_{\gamma 1} = 511$ keV and $E_{\gamma 2} = 1274$ keV. From this comparison we estimated that $\alpha \simeq 1.53$. Assuming proportionality (1), the value of FWHM, characterizing the spectrometer response function in $^{22}$Na measurements with optimally adjusted angles $\Phi = 87°$ and $\Psi = 68°$, should be equal to 127 ps. In contrast to this, the value of FWHM obtained from regular $^{22}$Na measurements, performed immediately after the above-outlined optimization with the aid of $^{60}$Co source, was found to be 144 ps. This discrepancy can be, at least in part, accounted for by a limited validity of proportionality (1) due to a non-linear response of the fast signal to the $\gamma$-ray energy (see Fig. 7) and by non-equivalent energy selections in two substantially different sets of measurements with $^{60}$Co and $^{22}$Na.

In routine measurements with the $^{22}$Na source, the energy windows of TSCAs in the slow branches of the spectrometer are precisely adjusted to include only the photopeaks at energies 511 and 1274 keV. Following our experience, the best choices of relative widths of the energy windows are 11 and 7% for the start and stop $\gamma$ rays with energies 1274 and 511 keV, respectively. In the regime of strobing the TAC with the signal derived from the $\gamma$-ray energy sum the relative position of the lower level of the window at the TSCA is chosen to be approximately 5% below the ideal energy sum. In addition, an energy pre-selection is used. For this sake the widths of the energy windows of CFDDs are set at minimum possible values that guarantee at the same time full overlapping with the corresponding windows of the TSCAs. The original purpose of this outlined pre-selection was to suppress the count rate of a priori useless fast signals at the outputs of CFDDs with the aim of achieving a lowered dead time of the main TAC. However, it turned out that such a pre-selection slightly improved the timing resolution and at the same time it became apparent that it also reduced parasite admixtures in delayed-coincidence spectra. The reason why the energy pre-selection is advantageous is as follows. Under conditions of a high count rate some slow signals at the inputs of the TSCAs result from a pile-up of the energies of *two* or *several* consecutive, closely spaced events of detection, so that energy selection, ensured by the TSCAs cannot work properly in these cases and a γ-cross talk may occur. On the other hand, signals at the inputs of CFDDs originate almost exclusively from *single* events of detection, not suffering from random pile-up.

In order to keep control over the overall quality of the spectrometer, special testing measurements of delayed-coincidence spectra are regularly carried out. In these cases, the adjustment of the spectrometer is the same as in the routine positron-lifetime experiments. For this purpose well-annealed pure α-Fe has been selected for reference samples. As this material is defect free, it is characterized by a single exponential component in the delayed-coincidence spectrum. Samples of α-Fe in the form of discs with dimensions $\varnothing 10\ \text{mm} \times 0.3\ \text{mm}$ are used. Apart from the determination of timing resolution power the purpose of testing measurements is (i) to check the correct functioning of the spectrometer by inspecting the deduced positron lifetime for α-Fe, (ii) to determine the detailed make-up of the time-resolution function, (iii) to estimate the contribution of the process of positron annihilation in the source material and the mylar foils to the delayed-coincidence spectrum, and (iv) to check for the absence of possible parasite structures or distortions in the measured spectrum by examining the degree of accordance between it and its model description. Over a period of more than 5 yr a series of these described testing measurements, with statistics typically $\geq 3 \times 10^6$ counts, yielded values for the positron lifetime in α-Fe that display fluctuations characterized by a standard confidence interval $108.1 \pm 0.2$ ps. It is to be noted that the values for this quantity known from the latest literature are 106 and 110 ps, see Refs. [19,20], respectively. It is to be stressed that a sample in which positrons annihilate predominantly with one characteristic lifetime, the value of which could be used as a precise and reliable standard, is still missing. An example of a positron-lifetime testing measurement with α-Fe is given in Fig. 11. The results deduced from this measurement are discussed in detail in Sections 5.2 and 5.3.

## 5. Performance

### 5.1. Energy resolution

Energy resolution, characterizing the quality of slow branches of the spectrometer, has been found to be 9.2% for $^{137}$Cs. This value, representing the FWHM of the 662 keV γ-line, has been obtained under conditions identical to those in routine positron-lifetime measurements, i.e. at room temperature, with a $^{22}$Na source strength of 1.3 MBq, with the same detector-source geometry and at the same shaping time of 0.25 μs, adjusted on SAs. For a weaker $^{137}$Cs source, with a larger shaping time of 1.5 μs and the temperature adjusted at $+3°$C, a record energy resolution of 6.8% has been observed, as illustrated in Fig. 12. The $^{137}$Cs γ-ray spectrum shown here is intentionally contaminated by $^{60}$Co lines to demonstrate a linear response of the slow signal to the γ-ray energy. To our knowledge, the best previous energy resolution was reported recently in Ref. [21] from the measurement of the $^{88}$Y γ-ray spectrum with a cylindrical $BaF_2$ scintillator of an enlarged thickness of 37 mm. For the same temperature $+3°$C the extrapolation from the data in Ref. [21] to the energy of 662 keV yields a FWHM of 9.5%.

### 5.2. Response function, timing resolution and related characteristics

Following our experience, the timing response function of the spectrometer can always be described as a superposition of three Gaussians. Initially, values of FWHM of these Gaussians were 135, 153 and $\simeq 800$ ps, their relative areas being $\simeq 50$, $\simeq 50$ and $< 0.2\%$, respectively. The FWHMs of the main two Gaussian were increasing during 3 yr of exploitation of the spectrometer up to values 155 and 175 ps for first and second one, respectively (see Section 6). In our approach the ratio of the relative contributions of two prominent gaussians is fixed, see Ref. [18]. Although the widest Gaussian contributes only weakly to the timing response function, its postulation is important in order to get a good agreement between the experimental delayed-coincidence spectra and their modelled counterparts. In the spectra with the total

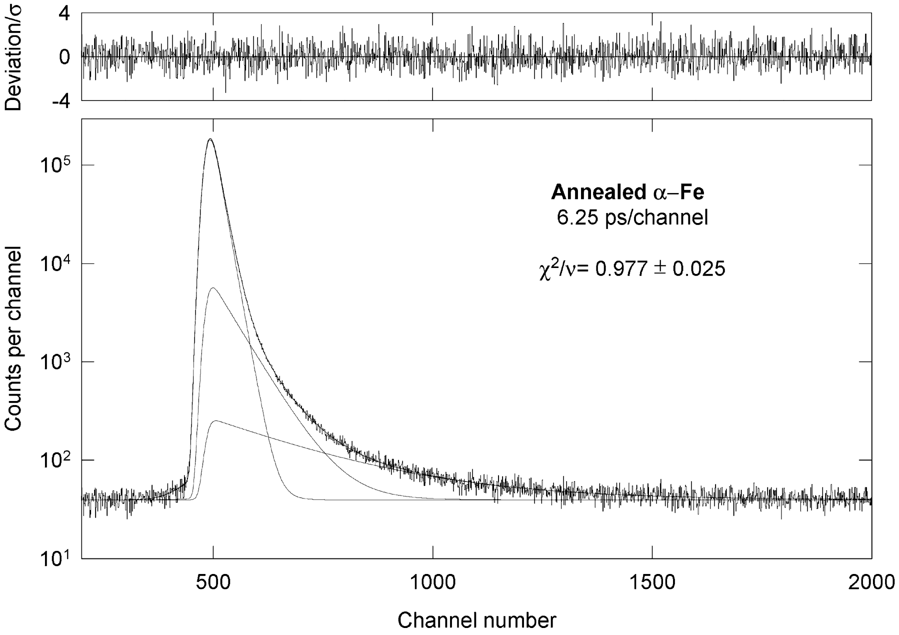

Fig. 11. An example of the α-Fe delayed-coincidence spectrum. The results of the decomposition of the spectrum into the individual positron-lifetime components, as well as the weighted residuals of the fit are also shown.

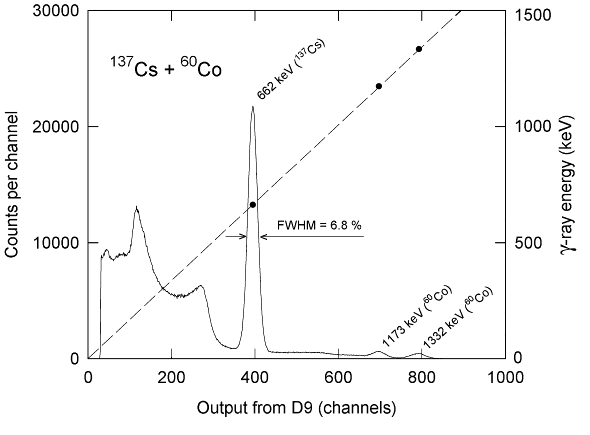

Fig. 12. The singles γ-ray spectrum of $^{137}$Cs measured with the BaF$_2$ detector at temperature $T \approx 3$°C.

number of counts exceeding $10^6$ the contribution of the widest Gaussian can be seen as a prelude of the main signal at the foot of its leading edge, see Fig. 11.

In order to understand better the makeup of the timing response function an auxiliary measurement of a delayed-coincidence spectrum with 0.2 MBq source of $^{60}$Co has been performed, see Fig. 13. Compared to $^{22}$Na delayed-coincidence spectra, the $^{60}$Co spectrum is expected to be formed only by the timing response function and some parasite component due to a γ cross talk. The parasite component is to be represented by a small, narrow, symmetrical and generally non-Gaussian peak that results from a convolution of the timing response function with the distribution for the time of flight of the cross-talk γ-rays, assuming that this time of flight is positive and negative for the scattering from the start detector to the stop detector and from the stop detector to the start detector, respectively. Following our estimates, the maximum range for the time of flight of scattered γ-rays is ± 150 ps. Under the strongly simplifying condition that the cross-talk time of flight is distributed uniformly within this range, our estimate for the upper limit of the FWHM of the parasite component in the $^{60}$Co spectrum leads to a value of 235 ps. As is

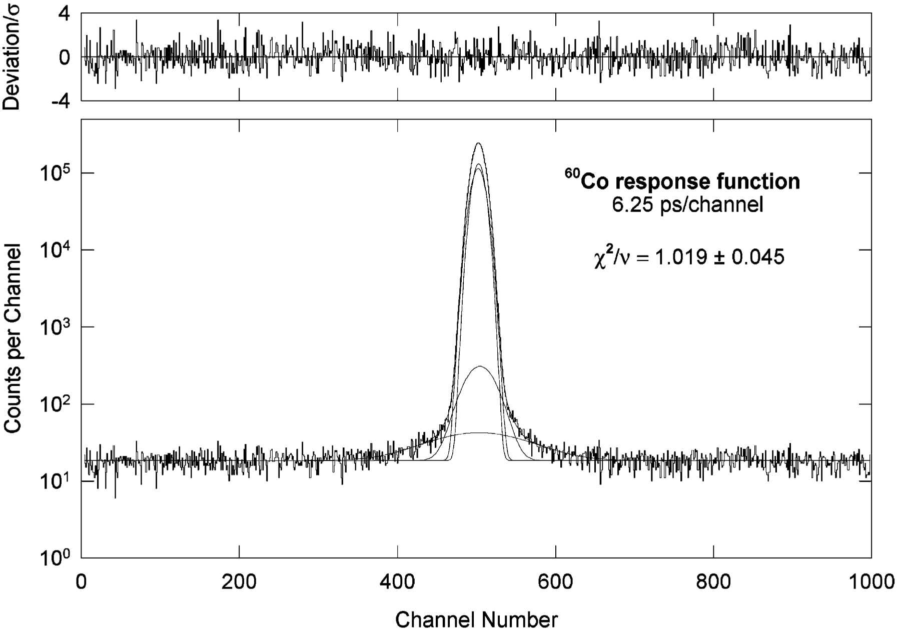

Fig. 13. A delayed-coincidence spectrum measured with a source of $^{60}$Co in the simplified mode of operation with the main TAC strobed autonomously, ignoring slow signals from dynodes D9. Energy windows of CFDDs were adjusted to include both $^{60}$Co lines at 1174 and 1332 keV. Individual smooth curves shown represent contributions of four gaussian parts superimposed on the time-independent background, as explained in the main text.

evident from Fig. 13, this spectrum obtained from our measurements can be decomposed into the following three parts: (i) the main component, formed by two equally intense Gaussians with FWHMs of 106 and 123 ps and an overall intensity of 99.6%, (ii) the 0.3% Gaussian component with a FWHM of 284 ps, and (iii) the 0.08% Gaussian component with a FWHM of 890 ps. Of these parts only the 284 ps Gaussian can be identified with the expected parasite component, belonging to the $\gamma$ cross-talk. Parts (i) and (iii) remain to be interpreted as constituents of the timing response function. The makeup of the response function in $^{60}$Co measurements thus strongly resembles that of the response function postulated in our approach to the analysis of $^{22}$Na delayed-coincidence spectra.

We attribute the widest Gaussians in $^{60}$Co and $^{22}$Na response functions to the random pile-up effects at the inputs of CFDDs; the pile-up meant in this context is that which comes from the summation of those parts of the fast signals that originate from the *fast*, 0.81 ns component of the scintillation light output. This explanation seems to be substantiated by the occurrence of the appreciably oscillating structures accompanying each fast signal. Such structures are apparent in Fig. 7. Another argument in favour of this explanation comes from the assertion that the relative size of the widest component of the response function increases with the increasing activity of the positron source. In this context it is to be noted that our attempts to understand the origin of the oscillations, accompanying the fast signals from dynodes D10, have not been successful. We have also failed to suppress them. Having in mind regular positron-lifetime measurements it is to be stressed that the considered widest component of the response function does not noticeably influence the extracted lifetimes nor the intensities of the individual lifetime components. It thus seems that oscillating trails of fast signals have no serious impact on the quality of measured delayed-coincidence spectra.

The above-mentioned part (ii) of the $^{60}$Co spectrum, attributed to the $\gamma$ cross-talk, is very small. It is therefore expected that the manifestation of the cross-talk process in regular positron-lifetime measurements with $^{22}$Na source should be beyond the threshold of observation. In particular, as follows from our crude assessment for the case of $\alpha$-Fe, the bias of lifetime estimates due to this $\gamma$ cross-talk is expected not be higher than 0.2 ps.

With the response function, represented by three Gaussians, the decomposition of the delayed-coincidence spectrum for $\alpha$-Fe (Fig. 11), mentioned in Section 4, led to the results that are summarized in column 3 of Table 2. Here, positron lifetimes $\tau$ and intensities $I$ of the individual components are listed. Quantities related to freely moving positrons are labeled by subscript f, while the source contributions are labeled by subscript s. The time-resolution function is characterized by values $w_1$, $w_2$ and $w_3$ of the FWHM for the three Gaussians. In the fitting procedure the distance between the centroids of the first two of them, $\delta_{1,2}$, is a free parameter, while the position of the remaining Gaussian is given by the weighted average of the positions of the first two. The ratio between areas of the first two Gaussians, say $A_1/A_2$, is fixed, while area $A_3$ of the third Gaussian is a free parameter. A constraint $A_1 + A_2 + A_3 = 1$ is assumed. The total FWHM is denoted by $w_{\mathrm{tot}}$. The last two rows of column 3 in Table 2 specify the quality of fit, represented by the sum of weighted squared residuals per degree of freedom, $\chi^2/\nu$, and the total number of counts.

Except for the main positron-lifetime component, belonging to the positron annihilation in the bulk $\alpha$-Fe, it is evident that two additional components are identified. They are attributed to the annihilation events coming from positron source material and its covering mylar foils. The spectrum of weighted residuals between the fitted and experimental data, shown in the upper panel of Fig. 11, does not indicate any traces of systematic difference between the experimentally measured delayed-coincidence spectrum and its description within the adopted model. Thus no noticeable distortions of the spectrum and, in particular, no apparent spurious short-lifetime components caused by detecting undesirable coincidence events [14,15]

Table 2
Results of analyses of delayed-coincidence spectra for $\alpha$-Fe and RPV-steel samples. These analyses were undertaken for the data taken before and after the recovery of the timing resolution power of the spectrometer. In parentheses standard deviations are shown in units of the last significant digit

| | $\alpha$-Fe | | RPV steel | |
|---|---|---|---|---|
| | May 1997 | November 1997 | May 1997 | November 1997 |
| $\tau_{\mathrm{f}}$ (ps) | 107.8(8) | 107.4(3) | 56(15) | 61(9) |
| $I_{\mathrm{f}}$ (%) | 93.4(2) | 93.3(2) | 10(1) | 13(1) |
| $\tau_{\mathrm{t}}$ (ps) | | | 147(3) | 151(2) |
| $I_t$ (%) | | | 81.2(8) | 79.8(8) |
| $\tau_{\mathrm{av}}$ (ps) | | | 137(4) | 139(3) |
| $\tau_{1,\mathrm{s}}$ (ps) | 367(7) | 373(6) | 340(14) | 358(15) |
| $I_{1,\mathrm{s}}$ (%) | 5.7(1) | 6.0(1) | 7.9(8) | 6.9(7) |
| $\tau_{2,s}$ (ps) | 1460(50) | 1640(70) | 1500(50) | 1430(60) |
| $I_{2,\mathrm{s}}$ (%) | 0.84(4) | 0.69(3) | 0.79(4) | 0.70(5) |
| $w_1$ (ps) | 152.6(3) | 138.4(6) | 150.4(5) | 138.0(8) |
| $w_2$ (ps) | 173(2) | 156(2) | 169(4) | 156(3) |
| $\delta_{1,2}$ (ps) | 50(2) | 28(2) | 49(3) | 27(3) |
| $w_{\mathrm{tot}}$ (ps) | 171 | 149 | 168 | 148 |
| $\chi^2/\nu$ | 1.037(24) | 0.986(24) | 1.026(24) | 0.955(24) |
| Counts | $7.8 \times 10^6$ | $7.8 \times 10^6$ | $8.4 \times 10^6$ | $8.3 \times 10^6$ |

seem to be created. With a $^{22}$Na source of activity 1.3 MBq the coincidence count rate reached in the fast–slow configuration of the electronics system is 35–40 $s^{-1}$, while for the alternative configuration [17] with the selection of $\gamma$-ray energy sum the count rate is typically $\simeq 75\ s^{-1}$.

### 5.3. An example of routine measurements

The present spectrometer has been designed mainly for the purpose of studying systems containing small-size defects. As demonstrated in our previous works [22–24], besides the components arising from positron trapping at defects, extremely short components with a few tens of picoseconds ascribed to free positrons can be identified. Recent measurements with a specimen of VVER-440-type reactor pressure vessel (RPV) steel 15Kh2MFA represent another example demonstrating such a capability.

The measured delayed-coincidence spectrum for this system is shown in Fig. 14. In contrast to the case of $\alpha$-Fe, the three-component model appears to be insufficient now. On the other hand, as can be seen from Fig. 14, the four-component model provides an excellent fit to the experimental data. In accordance with the results obtained for $\alpha$-Fe, the two longest components may easily be explained as those belonging to the contribution of mylar foils and the source material. The remaining two components with the shortest lifetimes thus have to be associated with positrons annihilating in the RPV steel. In fact, due to the complex structure of the steel material, the positron-lifetime spectrum is expected to contain more than two components. A detailed interpretation of the shape of the spectrum is, however, out of the scope of the present paper and we shall confine ourselves to a simplified approach assuming that the shorter component belongs to the annihilation of the delocalized positrons, while the longer one is attributed to the annihilation of positrons trapped at defect sites.

The results obtained with the RPV-steel and the well-annealed $\alpha$-Fe are compared in detail in Table 2. The meaning of some of the quantities shown in Table 2 is specified in Section 5.2. Quantities related to the trapped positrons within the above-outlined simplified picture are labeled by subscript $t$. The quantity $\tau_{av}$ stands for the average lifetime, i.e. $\tau_{av} = (I_f\tau_f + I_t\tau_t)/(I_f + I_t)$. The lifetime $\tau_t$ observed in the RPV steel (Table 2) agrees

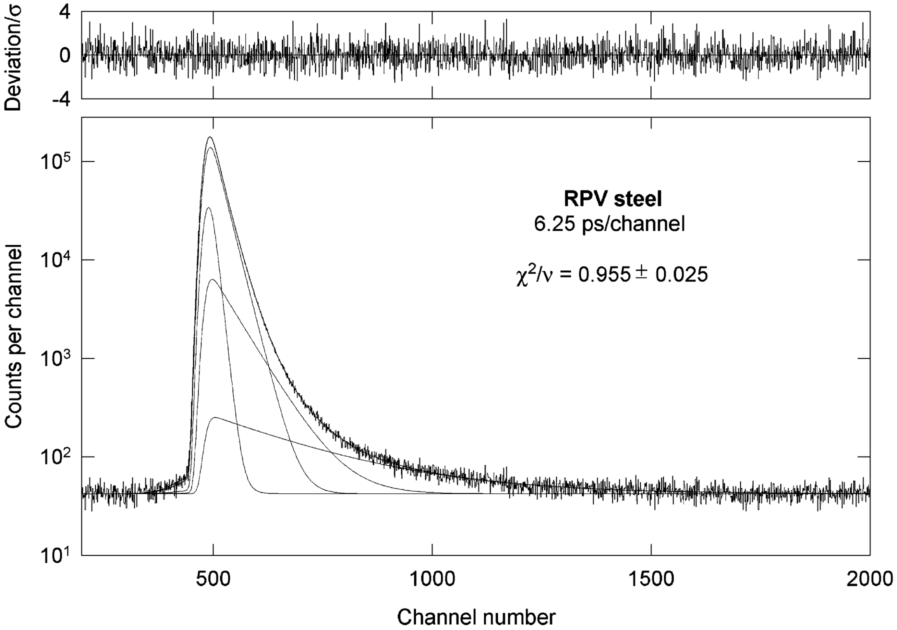

Fig. 14. An example of the RPV-steel delayed-coincidence spectrum. For details see the caption of Fig. 11.

reasonably well with the experimental values of $\simeq$ 150 ps reported earlier [25] for RPV steels of similar composition. As mentioned in Section 3.3, in the middle of 1997 the degradation of PMT gain and the timing resolution due to the ageing of the dynode systems was compensated for. The columns of the table, labeled as "May 1997" and "November 1997", illustrate quantitative difference between the timing resolution of the spectrometer before and after this remedy. Looking at the data in Table 2 from May 1997, it is evident that the three- and four-component fits to the $\alpha$-Fe and RPV-steel data, respectively, lead to mutually compatible values of parameters for the timing response function. The close quantitative agreement between the two sets of data on the response function is evident also from measurements with $\alpha$-Fe and RPV-steel samples after the improvement of timing resolution in November 1997. In connection with this it is to be noted that quantities $w_1, w_2$ and $\delta_{1,2}$ were always treated as free parameters. Bearing in mind the four-component fits of the RPV data, it is evident from Table 2 that two sets of measurements that differ in the spectrometer's resolution power lead to mutually consistent lifetime values and intensities of the individual positron groups. This kind of mutual agreement is also observed in the case of $\alpha$-Fe. At the same time the degree of accordance between the experimental and modelled delayed-coincidence spectra is characterized by almost ideal values of $\chi^2/v$ for a broad range of the time scale, including the leading edge of the "true" delayed-coincidence signal. Taking into account the relatively high numbers of recorded events of annihilation, these conclusions represent another piece of indirect evidence in favour of the accuracy of the adopted model for the spectrometer's response function and the absence of parasite structures in the delayed-coincidence spectra.

## 6. Experience with long-term exploitation of the Spectrometer

### 6.1. The use of high-voltage dividers I–III

Our testing of a provisional version of the spectrometer led us to guess that to get the maximum timing resolution it was important to apply maximum voltages between the photocathode and the first dynode D1, between D1 and D2 and possibly between D2 and D3. This finding has been taken into account in the design of all the HV dividers reported in this paper. The justification of these increased voltages can easily be understood if the relative variance of the number of emitted secondary electrons decreases with their increasing average.

As is evident from Fig. 15, the use of the HV divider I resulted in an excellent initial timing resolution, represented by a FWHM of 142 ps, as deduced from standard testing measurements with $\alpha$-Fe. Unfortunately, the resolution of the spectrometer turned out to be subject to gradual worsening. Besides that, we observed a drastic systematic decrease of the sizes of slow signals from both photomultipliers. Though the use of modified HV dividers II and III slightly influenced the rate of worsening of the timing resolution, as well as the decrease of slow signals, it became evident that these dividers did not bring a radical solution of the problem. In fact, as can be seen from Fig. 15, any of the dividers I–III combined with the photomultipliers of later production (ser. Nos. 40423 and 40436) were not acceptable, as they guaranteed a life span of the spectrometer which could only be measured in months, rather than in years.

Comparison between the rates of degradation, apparent in Fig. 15, provides some guidelines for better understanding the nature of the observed effects. If the systematic decrease of the PMT signals were connected exclusively with a degradation of the photocathode quantum efficiency, one would have observed a much larger degradation of the timing resolution. Indeed, assuming the $N_{\mathrm{pe}}^{-1/2}$ law, in the case of divider I the observed increase of the FWHM from 148 to 159 ps would have been accompanied with a decrease of the slow signal characterized by a factor of 0.87, and not $\simeq 0.62$ or $\simeq 0.68$, as it was actually observed for a given pair of PMTs. This discrepancy, and also the fact that the rate of decrease of the slow signal apparently depended on the voltage distribution along the dynode chain, led us to surmise that the primary source of difficulties with timing resolution was a gradual decrease of the PMT gain. Such

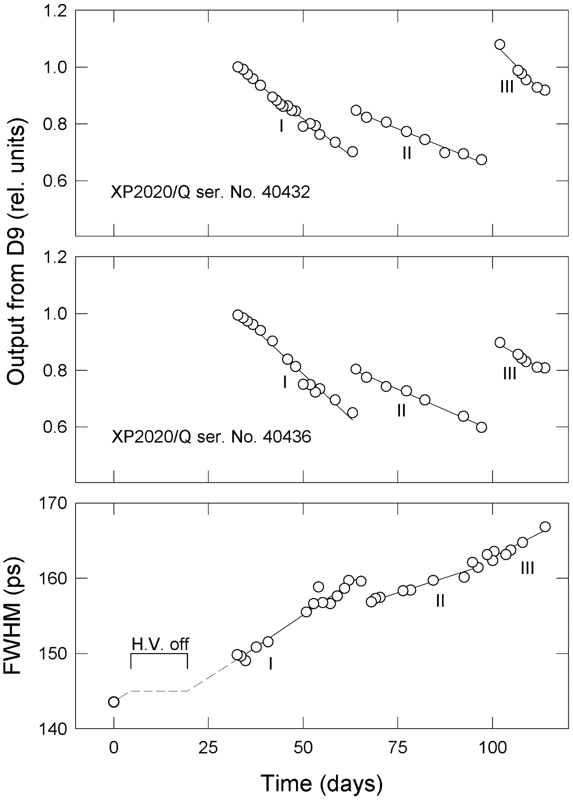

Fig. 15. Timing resolution and sizes of slow output signals as functions of time for the spectrometer for the cases of HV dividers I–III

degradation can be attributed to irreversible changes of coefficient of secondary electron emissions from several of the last dynodes due to the long-lasting exposure of dynodes to electron bombardment. If the coefficient of secondary emission changes, the shapes of fast-output signals from dynodes D10 will necessarily change too. Specifically, with lowering this coefficient the size of the leading negative part of the fast signal increases relatively to that of the positive part. As is evident from Section 3.3, in the case of both detectors the fast signal is inverted before it reaches the input of the CFDD, so that it is the positive part of the original signal that is mainly responsible for exciting the CFDD. Nevertheless, as the resulting zero-crossing timing is also influenced by the leading negative part of the original fast signal, the changes in proportions of the positive and negative parts alter the detector timing properties.

## *6.2. The use of high-voltage dividers IV*

### *6.2.1. PMT gain*

As an important step in upgrading the performance of the spectrometer, the HV dividers IV were installed and the PMTs of more recent production were replaced by those produced before 1986 (see Section 3.1). The data in Fig. 16 indicate that these measures turned out to be successful, as they reduced the initial rate of systematic decrease of the PMT gain. Moreover, for both detectors the observed size of the signal from dynode D9 as a function of time displayed a very obvious tendency to saturate. As a result, the overall decline of slow signals we observed over the period of 4.3 yr is represented by a factor not lower than 0.09. This contrasts with the result of our extrapolation of data in Figs. 16 and 17, according to which such an attenuation would have been reached with dividers I and the PMTs of more recent production sooner than after 6 months. As far as fast signals are concerned, with dividers IV after 4.3 yr of operating the spectrometer they decreased by a factor of $\simeq 0.25$, eventually becoming too small to excite the CFDDs. This decrease is markedly lower than that of the slow signals, which is a consequence of saturation of the *fast component* of fast output signals due to the effects of space charge.

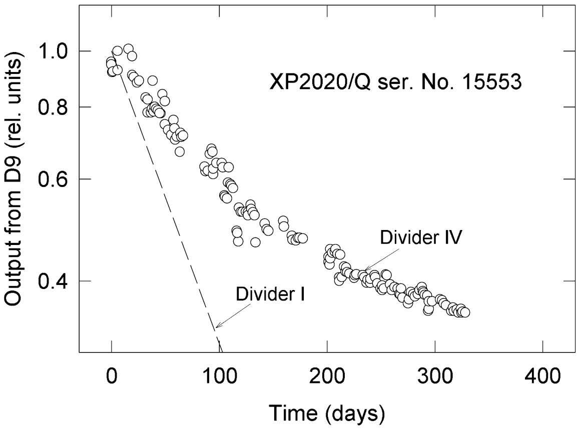

Fig. 16. The output from dynode D9 of PMT ser. No. 15553 as a function of time for the case of divider IV (circles). Behaviour of analogous output from a PMT of later production (ser. No. 40432), equipped with divider I, is shown for comparison (broken line).

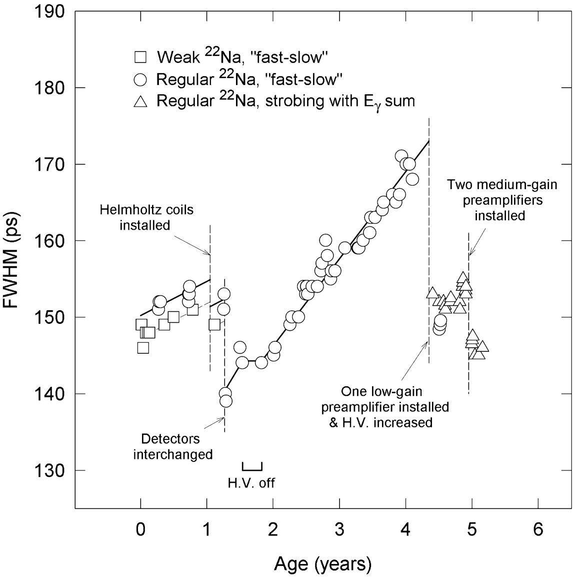

Fig. 17. Timing resolution as a function of time for the spectrometer equipped with the HV dividers IV.

It seems plausible that the loss of ability of a dynode to emit secondary electrons is proportional to the product of the total number of primary electrons and some *increasing* function of their kinetic energy. Accepting this possibility it might appear that the achieved low rate of degradation of the PMT gain is mainly due to a strong suppression of the inter-dynode voltages at the end of the dynode chain. However, closer analysis suggests to our surprise that this expectation is justified only for the gain of the last dynodes, but not for the gain of the *whole* active dynode system.

Let us consider the coefficient of secondary emission $q_i$ from the $i$th dynode that is proportional to the voltage $U_i$, applied between this dynode and the preceding electrode, and also to a factor of deterioration $f_i$, i.e.

$$q_i = aU_i f_i. \tag{2}$$

Considering a *pristine* PMT, the constant of proportionality $a$ is common to all dynodes. For the sake of simplicity let us further assume that

$$f_i = 1 - \kappa t U_i \bar{I}_i. \tag{3}$$

Here, $\kappa$ is another constant of proportionality, $\bar{I}_i$ the average current of primary electrons to the $i$th dynode and $t$ the elapsed time. Expressing $\bar{I}_i = \bar{I}_0 G_{i-1}$, where $G_j$ is the gain of the PMT at the $j$th dynode and $\bar{I}_0$ the average photocathode current, for small values of $t$ the PMT gain at the $n$th dynode is

$$G_n = \prod_{i=1}^{n} aU_i\left(1 - \frac{\kappa t \bar{I}_0}{a}\prod_{j=1}^{i} aU_j\right). \tag{4}$$

Using this expression it can easily be shown that the initial *relative* loss of the gain per unit of time is

$$\left(\frac{1}{G_n}\frac{\mathrm{d}G_n}{\mathrm{d}t}\right)_{t=0} = -\frac{\bar{I}_0\kappa}{a}\sum_{i=1}^{n}(G_i)_{t=0}. \tag{5}$$

From this expression it is evident that for a fixed value of $G_n$ the suppression of inter-dynode voltages at the end of the dynode chain in fact *enhances* the rate of the gain degradation. It is believed that this qualitative conclusion is valid not only in idealized conditions, but also in the case of the real behaviour of quantities $q_i$ and $f_i$. The suppressed degradation of gain $G_9$ seen in Fig. 16 for the combination of the PMT of older production with the HV divider IV thus seems to be a result of the extremely good quality of dynode surfaces of the PMT used, not a result of the changed inter-dynode voltages.

### 6.2.2. The timing resolution

The most important outcome of the combination of dividers IV with the older PMTs is the radical solution to the above-mentioned problem of timing resolution, which is apparent from Fig. 17. The lowered inter-dynode voltages, provided by these dividers, lead to low secondary emissions from the last dynodes. As a consequence, the absolute values of integrals over the positive and negative parts of the fast signal are almost the same, see Fig. 7. Since the front edge of the leading negative part of each such signal is out of the reach of the positive part, the changes of the coefficients of secondary emission $q_i$ from the last dynodes should not have any direct impact on the timing resolution power of the spectrometer, not mentioning that these changes are small. This is evidently not the case with dividers I–III. However, the systematic deterioration of overall PMT gain $G_{10}$ at dynodes D10 still brings some difficulties. Specifically, in view of the decreasing role of saturation due to the space-charge effects, the shape of the negative part of the fast signal inevitably changes. In addition, these signals become too small to be processed by the CFDDs without some influence of a non-negligible level of electronic noise. For these reasons, if operation conditions remain unchanged, the value of the FWHM will systematically increase with the effective time of running the spectrometer. Nevertheless, as can be seen from Fig. 17, this crucial quantity was found to be still stable enough within a period of 4.3 yr without the need for a remedy. It is interesting to note that in the case of dividers I and PMTs of newer production the rate of worsening of the timing resolution is higher by a factor of 20, see Figs. 16 and 18.

### 6.3. *Compensating the effects of ageing*

During an almost continuous exploitation of the spectrometer lasting more than five years several compensation measures were undertaken to improve the otherwise slowly worsening timing resolution. As is evident from Fig. 17, a remarkable lowering of the value of the FWHM, characterizing this resolution, has been achieved by interchanging the “start” and “stop” detectors. Referring to a note in Section 4, this improvement was achieved thanks to the use of a detector with better timing properties for the detection of 511 keV $\gamma$ rays. Also mounting the Helmholtz compensating coils led to some improvement in resolution. Unfortunately, both these compensating measures for better resolution could be undertaken, in principle, only once. On the other hand, provided that there exists a link between the gradual loss of the fast signals and the worsening of the timing resolution, as outlined in Section 6.2.2, the remedy can be *repeatedly* achived by increasing the high voltage and/or the gain of the high-frequency amplifiers. With this perspective the lifespan of the spectrometer seems to be still far from expiry. From the data in Fig. 17 it is evident that the increase of the high voltage from 2450 to 2500 V and the installation of two single-chip 1.8 GHz amplifiers with a gain of 11 dB (see Section 3.3) restored the timing resolution almost to its initial status.

### 6.4. *Other relevant details*

During the long-term exploitation of the spectrometer we found that the ageing process did not affect the optimum rotation angles of the detectors. Similarly, optimum voltage differences between pairs of electrodes g1-K and D2-D1 also turned out to be intact despite ageing. Our success in restoring the timing resolution strongly indicates that no degradation of quality of $BaF_2$ crystals or their optical coupling with photocathodes took place and that the quantum efficiency of the photocathodes of both PMTs used remained stable, notwithstanding the fact that the detector system was exposed to an environment strongly polluted by He gas. It may be that the endurance of our system was achieved owing to the fact that the $BaF_2$ crystal and the PMT of each detector was encapsulated in a carefully sealed common housing.

The data in Fig. 17 indicate that the use of positron sources of lower activities leads to a slightly better timing resolution. Specifically, the decrease of activity from its standard value of 1.3 to 0.5 MBq improved the resolution by about 2–3 ps. This improvement can be accounted for by the suppressed probability of a pile-up of the fast-output signal originating from the 0.81 ns scintillation component with the fast-output signals belonging to the *slow*, approximately 1 μs component [13]. On the other hand, a small decline in timing resolution, characterized by a 1–2 ps increase of FWHM, was observed when we started to work in the strobing regime with the $\gamma$-ray energy sum. The reason for this increase is not yet understood.

## 7. Concluding remarks

The described spectrometer was assembled almost exclusively from materials, components and modules that were commercially available. Notwithstanding this fact, the spectrometer's performance, described in Sections 5 and 6.2, as well as by its successful long-term behaviour, seems to convincingly exceed current standards for similar equipments. Its noteworthy features are as follows: (i) the superior timing resolution, (ii) the simple make-up of the response function, (iii) a virtual absence of parasitic components and distortions in the measured delayed-coincidence spectra, even under conditions when the overall number of recorded events exceeds $10^7$, and (iv) a fully acceptable throughput, especially in the mode of operation of strobing by the $\gamma$-ray energy sum. In our experience the most crucial measures that lead to the achieved performance of the spectrometer are:

- high-quality PMTs are used (see Section 3.1),
- the PMT with the best timing properties is employed for detection of the 511 keV $\gamma$ rays (Sections 4 and 6.3),
- the dynode timing derived from the negative, "anode-like" component of the PMT fast signal is used (Section 3.2),
- an increased HV is applied at the beginning of the dynode chains, while the inter-dynode voltages at the last stages of the chains are lowered (Section 3.2),
- $BaF_2$ crystals are protected against moisture (Section 3.1),
- the choosen detector–source geometry reduces the simultaneous detection of two 511 keV $\gamma$ rays (Section 4),
- angular positions of PMTs are carefully optimized (Section 4), and
- high-frequency, single-chip preamplifiers are used to enhance PMT fast signals (Section 3.3).

We believe that our reported timing resolution is still not the utmost limit for a given class of detectors, formed by $BaF_2$ scintillators and Philips XP2020/Q PMTs. Referring to the discussion in Section 4 it seems that with PMTs of qualities close to those of the PMT in our stop detector a value of FWHM lower than 130 ps can be reached.

## Acknowledgements

The authors are greatly indebted to Mrs. E. Doušová for her assistance in mounting the scintillation crystals and also to Drs. Y. Jirásková and J. Kočík for their preparation of samples of α-Fe and RPV steel. Financial support received from Charles University (Grants № 285/93 and № 160/95) in the initial stages of this work and from The Grant Agency of the Czech Republic (Grant No 106/96/1319) during the final period of the work are gratefully acknowledged.

## References

[1] A. Dupasquier, A.P. Mills, Jr. (Eds.), Positron Spectroscopy of Solids, Proceedings International School of Physics "Enrico Fermi", Course CXXV, Varenna 1993, IOS Press, Amsterdam, 1995.

[2] M. Laval, M. Moszyński, R. Allemand, E. Cormoreche, P. Guinet, R. Odru, J. Vacher, Nucl. Instr. and Meth. 206 (1983) 169.

[3] W. Bauer, J. Major, W. Weiler, K. Maier, H.E. Schaefer, in: P.C. Jain, R.M. Singru, K.P. Gopinathan (Eds.), Proceedings 7th International Conference on Positron Annihilation, World Scientific, Singapore, 1985, p. 804.

[4] H. Rajainmäki, Appl. Phys. A 42 (1987) 205.

[5] B. Bengtson, M. Moszyński, Nucl. Instr. and Meth. 204 (1982) 129.

[6] J. de Vries, A. Zecca, R.S. Brussa, R.G. Grisenti, S. Oss, Nucl. Instr. and Meth. A 275 (1989) 194.

[7] J. de Vries, F.E.T. Kelling, Nucl. Instr. and Meth. A 262 (1987) 385.

[8] J. de Vries, Ph.D. Thesis, Delft University of Technology, Delft, 1987.

[9] T. Chang, D. Yin, C. Cao, S. Wang, J. Liang, Nucl. Instr. and Meth. A 256 (1987) 398.

[10] P. Sperr, Nucl. Instr. and Meth. A 254 (1987) 635.

[11] F. Bečvář, L. Lešták, I. Novotný, I. Procházka, F. Šebesta, J. Vrzal, Materials Science Forum 175–178 (1995) 947.

[12] Photomultiplier Tubes, Principles & Applications, Philips Photonics, Hamburg, 1994.

[13] D.F. Anderson, D.C. Lamb, Nucl. Instr. and Meth. A 262 (1987) 377.

[14] R. Simon, private communication (1991).

[15] T. Goworek, W. Górniak, J. Wawryszczuk, Nucl. Instr. and Meth. A 321 (1992) 129.

[16] B. Bengtson, M. Moszyński, Nucl. Instr. and Meth. 204 (1982) 129.

[17] F. Bečvář, J. Čížek, I. Procházka, Acta Phys. Polonica A 95 (1999) 448.

[18] I. Procházka, I. Novotný, F. Bečvář, Mater. Sci. Forum 255–257 (1997) 772.

[19] A. Seeger, F. Banhart, Phys. Stat. Sol. (a) 102 (1987) 171.

[20] A. Vehanen, P. Hautojärvi, J. Johansson, J. Yli-Kaupilla, Phys. Rev. B 25 (1982) 762.

[21] V. Nanal, B.B. Back, D.J. Hofman, Nucl. Instr. and Meth. A 389 (1997) 430.

[22] Y. Jirásková, O. Schneeweiss, M. Šob, I. Novotný, I. Procházka, F. Bečvář, B. Sedlák, J. Phys. IV (suppl. J. Phys. III) C1 5 (1995) 157.

[23] P. Čada, M. Cieslar, P. Vostrý, F. Bečvář, I. Novotný and I. Procházka, Acta Phys. Pol. A 88 (1995) 111.

[24] J. Čížek, I. Procházka, P. Vostrý, F. Chmelík, R.K. Islamgaliev, Acta Phys. Polonica A 95 (1999) 487.

[25] G. Brauer, L. Liszkay, B. Molnar, R. Krause, Nucl. Eng. Des. 127 (1991) 47.